Probing the effect of different exchange-correlation functionals on the optoelectronic features of chalcogenide compound Ag_2O

H. Mancer

Hassiba Benbouali University of Chlef, Faculty of Exact-Sciences and Informatics, Department of Physics, Chlef, Algeria.
Hassiba Benbouali University of Chlef, Faculty of Exact-Sciences and Informatics, Laboratory for Theoretical Physics and Material Physics, Chlef, Algeria.

M. Caid

Djillali Liabes University of Sidi Bel Abbès, Faculty of Exact-Sciences, Magnetic Materials Laboratory, Sidi Bel-Abbès, Algeria.
Ecole Normale Supérieure de Bou-Saâda, Département des Sciences Exactes, Bou-Saâda, M'sila, Algérie.

H. Rached

Hassiba Benbouali University of Chlef, Faculty of Exact-Sciences and Informatics, Department of Physics, Chlef, Algeria.
Djillali Liabes University of Sidi Bel Abbès, Faculty of Exact-Sciences, Magnetic Materials Laboratory, Sidi Bel-Abbès, Algeria.

Z. Nakoul

Djillali Liabes University of Sidi Bel Abbès, Faculty of Exact-Sciences, Magnetic Materials Laboratory, Sidi Bel-Abbès, Algeria.

D. Rached

Djillali Liabes University of Sidi Bel Abbès, Faculty of Exact-Sciences, Magnetic Materials Laboratory, Sidi Bel-Abbès, Algeria.

Received 7 April 2022; accepted 20 June 2022

The primary goal of this study is to investigate the effect of different exchange-correlation functionals on the optoelectronic and elastic properties of the Ag_2O chalcogenide compound. For the electronic structures and optical spectra, the Tran-Blaha modified Becke-Johnson approach combined with GGA and GGA+U (mBJ-GGA-PBEsol and mBJ-GGA-PBEsol+U, respectively) was used. The available theoretical and experimental data for the bandgap energy were reported to determine whether there is a correlation with our results. The electronic structure revealed that our compound is a direct semiconductor at the R-symmetry point with a bandgap of 1.22 eV, which agrees well with the experimental values for the first time. The elastic constants were also evaluated using the IRelast package, which revealed that the compound was mechanically stable. Finally, the optical response was systematically studied, and it was found that Ag_2O exhibited excellent optical efficiency.

Keywords: Chalcogenide compounds; *mBJ-GGA-PBEsol+U*; electronic structures; optical response; DFT calculations.

DOI: https://doi.org/10.31349/RevMexFis.69.011004

1. Introduction

Binary silver oxide is an isostructural compound that crystallizes in the Cu_2O cuprite structure within the $Pn\bar{3}m$ space group (224) [1,2], which is a semiconductor material. Tjeng *et al.*, have experimentally explored the electronic structures of the Ag_2O compound and reported a bandgap of 1.3 eV [3]. Silver oxide has been widely studied owing to its many important applications, such as in solar energy converters [4], battery technology [5-8], antibacterial applications [9-11], and molecular sensor technology [4], for example, as an enzyme-free glucose sensor with Cu [4,12]. It has also been reported that Ag_2O can be employed in water splitting [13], optical memory [14], photography [15], organic catalysis, such as transmetalation [16], and the oxidation of aldehydes by molecular oxygen [17]. The remarkable properties of Ag_2O which have important roles in fast-ion-conducting glasses of AgI-Ag_2O-B_2O_3, AgI-Ag_2O-V_2O_3, and AgI-Ag_2O-P_2O_5 are the negative thermal expansion behavior of the cuprite Ag_2O and the structural phase transition that occurs at 35 K [18-23].

In the literature, many theoretical methods within different approximations have been employed to accurately describe the different properties of this material. F. Pei *et al.*,

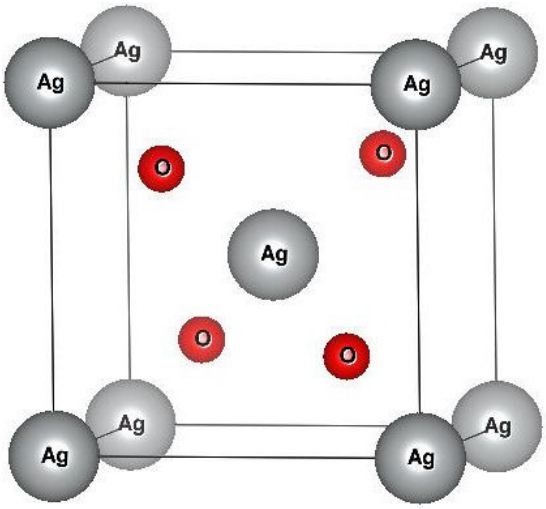

FIGURE 1. The Ag_2O compound with cuprite structure.

[24], used the plane-wave-pseudopotential method as incorporated in the CASTEP code to study the structural, electronic, and optical properties of Ag_2O with cubic cuprite structure. Jeremy P. Allen *et al.*, [25], have described the electronic structure of Ag_2O using various calculation methods. The structural, electronic, elastic, thermal, and optical properties of Ag_2O were also investigated using the Wien2k code with different approximations (LDA, GGA, Engel-Vosko-GGA, and modified-Becke-Johnson-GGA) by Haleem Din and A. H. Reshak [26]. Using the projector-augmented-wave pseudopotentials as incorporated in the VASP code within LDA and LDA+U approximations, Naoto Umezawa *et al*. [27], have studied the electronic structures of Ag_2O compound. As presented previously, numerous theoretical calculations of the electronic structures have been reported for this material but, none of them has exact bandgap energy compared to the experimental ones. To resolve this discrepancy, we used a new exchange-correlation functional for the mBJ potential coupled with Hubbard correction in the framework of the DFT-theory. The main objective of this study is to provide a better description of the electronic structure and optical spectra of the chalcogenide compound Ag_2O.

2. Calculation method

In all our calculations, we used the FP-LAPW method [28,29], based upon the DFT-theory [30,31], and executed in the Wien2k code [32]. The muffin-tin sphere radii (R_{MT}) for Ag and O are 1.96 and 1.69 (a.u), respectively. The input parameters such as $R_{MT} \times K_{\max}$, $G_{\max}$, and cut-off energy are respectively 7, 12 $Ry^{1/2}$, and -7 Ry, where $K_{\max}$ is the maximum modulus for the reciprocal lattice vector, R_{MT} is the smallest atomic sphere radius, cut-off energy is the separation energy between the valence and core states, and $G_{\max}$ defines the magnitude of the largest vector in the charge density Fourier expansion. The Monkhorst-Pack method in the first Brillouin zone (BZ) was performed using 1000 *k*-points. Regarding the atomic positions, the Ag_2O contains two atoms, where the Ag and O atoms occupy (0,0,0) and (1/4,1/4,1/4), respectively, as shown in Fig. 1.

GGA-PBEsol-mBJ and GGA-PBEsol-mBJ+U were used to determine the optoelectronic properties. The U values were taken as $U^1 = 5.8$ eV [3], and $U^2 = 11.2$ eV [33] for Ag-$4d$. The elastic properties of the Ag_2O compound were studied using the IRelast package [34,35] within the GGA-PBEsol approach.

3. Results and discussion

3.1. Equilibrium ground-state and electronic structures

The equilibrium lattice constant a_0, bulk modulus B_0, and its pressure derivatives, were obtained by fitting the total energy as a function of the unit-cell volume using Murnaghan's equation of state [36]. In this way, the volume optimization is carried out by minimization of the total energy versus volume. The obtained results of a_0(Å) and B_0(GPa) are given in Table I with some other available theoretical and experimental results for comparison. This table shows that the a_0 and B_0 for Ag_2O are consistent with the available theoretical and experimental results.

To explore the electronic behavior of the studied compound, we calculated the density of state DOS and electronic band-structure BS along with the principal symmetry points in the BZ for the cuprite structure (X-R-M-Γ-R) using the GGA-PBEsol-mBJ and GGA-PBEsol-mBJ+U for the exchange-correlation functional (see Fig. 2). The result of BS reveals the semiconductor nature with a direct bandgap at the R-symmetry point. The distinct features noticed within GGA-PBEsol-mBJ compared to GGA-PBEsol-mBJ+U shifts the conduction band upward and increase the bandgap.

TABLE I. The calculated lattice constant a_0(Å) and bulk modulus B_0(in GPa) for the Ag_2O compound.

Compound	a_0(Å)			B_0(GaP)		
	This work	Exp.	Theor.	This work	Exp.	Theor.
Ag_2O	4.714	4.74 [37]	4.73 [26]	90.81	-	86.73 [26]
		4.718 [33]	4.81 [24]			74.0 [24]
			4.83 [37]			

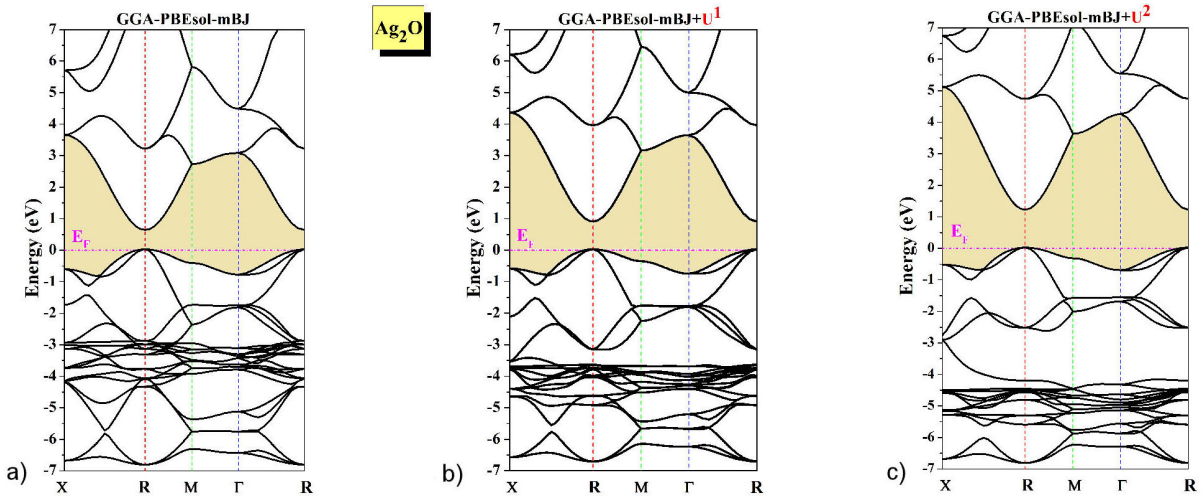

FIGURE 2. The calculated band structure of Ag_2O compound using: a) mBJ-GGA-PBEsol, b) mBJ-GGA-PBEsol+U^1, and c) mBJ-GGA-PBEsol+U^2 approaches.

TABLE II. The Calculated bandgap (in eV) of Ag_2O compound.

Compound	The bandgap (eV)		
	This work	Exp.	Theor.
Ag_2O	1.22	1.24 [33]	0.63 (mBJ) [26]
		1.30 [3]	0.41 (EV-GGA) [26]
		1.40 [38]	0.176 (GGA) [26]
			0.155 (LDA) [26]
			0.17 (LDA+U) [27]

The overall bandgap result of GGA-PBEsol-mBJ is better than that of other theoretically calculated bandgaps (LDA, GGA, EV-GGA, and LDA+U) [26,27], but significantly underestimated the bandgap from the experimental values as shown in Table II. Whereas, to resolve this discrepancy of bandgap and provide a value almost comparable to the experimental data, we used the GGA-PBEsol-mBJ+U. It should be noted that the obtained value is consistent with the experimental values for the first time. Furthermore, the conduction-band-minimum CBM shifts towards higher energy compared to the GGA-PBEsol-mBJ position, but the position of the valence-band-maximum VBM remained fixed.

Total and partial DOS (TDOS and PDOS, respectively) calculated using GGA-PBEsol-mBJ+U^2 are shown in Fig. 3. The DOS spectra are divided into four regions. The First region, situated between (-6.7 and -5.8 eV) is a result of mixed Ag-4*d* and *O-2p* states. The lower limit of this region also includes a small amount of Ag-*5s* states. The second one located between (-5.8 eV and -2.7 eV) is dominated principally by Ag-*4d* states, with a minority of O-*2p* states. The third region below the Fermi level (E_F) consists of mixed Ag-*4d* and O-*2p* states, with a small contribution from Ag-*5s*. The bottom of the conduction band is mainly composed of Ag-(*5s*,*5p*) and O-(*2s*,*2p*) states.

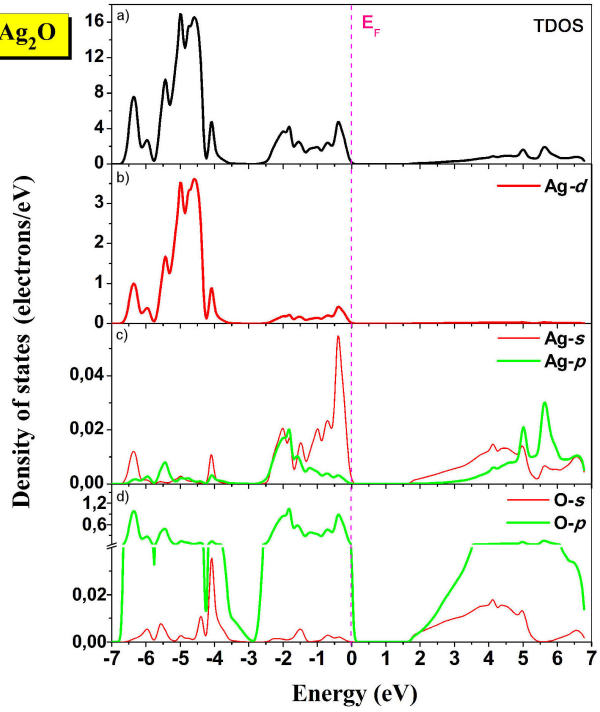

FIGURE 3. The calculated total and partial density of states for Ag_2O compound using the mBJ-GGA-PBEsol+U^2 approach.

3.2. Elastic properties

The calculation of elastic properties is important to obtain more information about the compound, such as mechanical stability, anisotropic binding character, bonding forces, and brittle or ductile nature. For cubic Ag_2O, the number of elastic constants is reduced to only three independent elastic parameters: C_{11}, C_{12}, and C_{44} (cubic crystals). The estimated values of these constants are useful for obtaining information about mechanical behavior. The calculated elastic constants are listed in Table III. We can see clearly that the obtained

TABLE III. The Calculated elastic constants $C_{ij}(C_{11}, C_{12}, C_{44})$, Bulk modulus (B), shear modulus (G), Young's modulus (E) (in GPa), Pugh's ratio (B/G), Poisson's ratio (ν) and anisotropy factor (A) of Ag_2O compound

Compound		C_{11}	C_{12}	C_{44}	B	G	E	B/G	A	ν
Ag_2O	This work	106.69	84.54	51.14	90.81	30.04	81.16	3.02	4.61	0.35
	Theor. [26]	132.36	70.94	56.18	86.73	44.093	113.11	1.967	1.829	0.282

C_{ij} satisfies the three well-known Born-Huang stability criteria for the cubic system [39], which means our material is mechanically stable. It is well-known that the anisotropy factor (A) is an important mechanical parameter for technological and engineering applications and for detecting micro-cracks in materials. If the anisotropy factor is equal to unity, the material is isotropic and for any value different from unity the material is anisotropic.

The anisotropy factor value is found to be 4.61 which indicates that the compound is an anisotropic material. For more information about the compound such as stiffness, type of bounds, hardness, and ductility (brittle), we have estimated the macroscopic mechanical moduli such as Young's modulus (E), Shear modulus (G), Pugh's ratio (B/G) and Poisson's ratio (ν). For that, we have applied the Voigt-Reuss-Hill approximation [40,41].

The calculated G_V, G_R, and G are 35.11, 24.98, and 30.04 GPa, respectively. Young's modulus (E) provides information about the stiffness of materials. For the higher value of $E = 81.16$ GPa, the material shows high stiffness. In addition, Poisson's ratio (ν) provides information about the bonding forces [42]. The central forces in the solid are trapped between 0.25 and 0.5, for the studied compound, we found $\nu = 0.35$. Due to this value, we can state that this compound is characterized by a metallic bonding. The two traditional parameters, Pugh's ratio of ductility and Poisson's ratio [43,44], are responsible for the brittle or ductile of a material. The calculated B/G and ν are 3.02 and 0.35, respectively. We can classify from these calculated values the investigated compound as ductile material. Table III displays our results of elastic constants and elastic moduli with other reported theoretical results. We can observe a significant deviation compared to our results, which is mainly due to the difference in the employed approximation.

3.3. Optical properties

To obtain more information about the electronic structure, we calculated the complex dielectric function $\epsilon(\omega)$. More descriptions of the optical calculation can be found in Ref. [45].

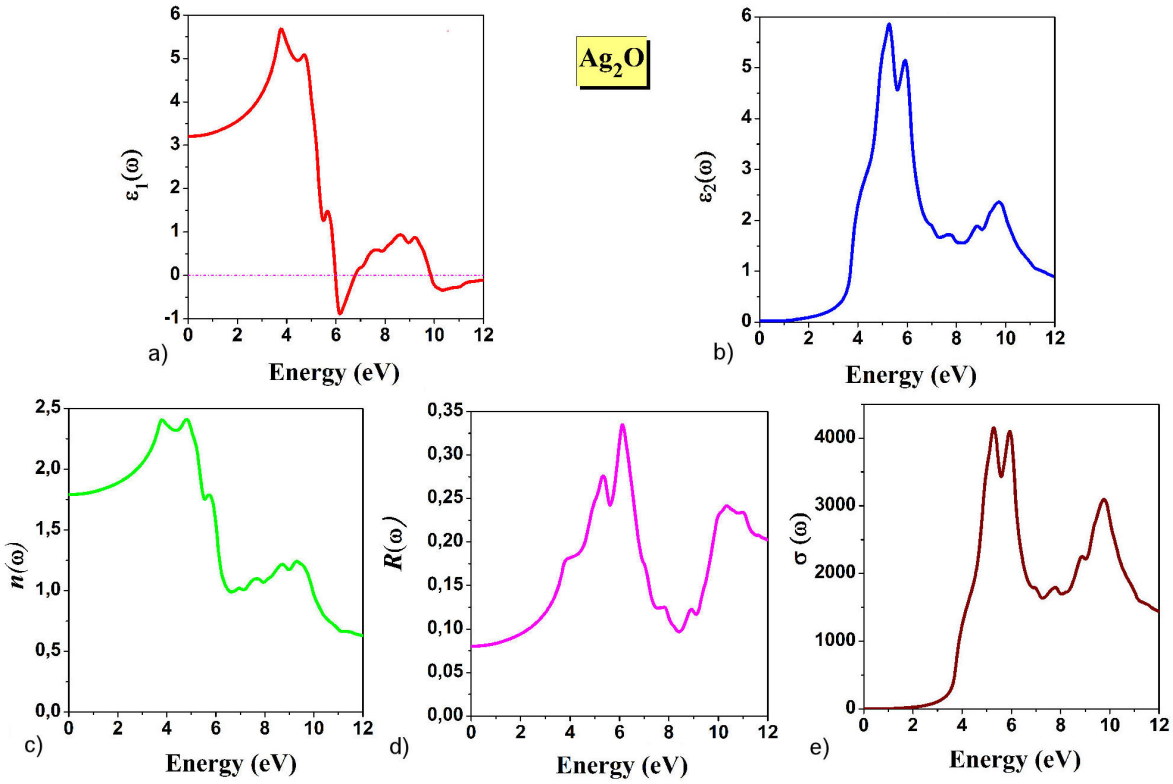

FIGURE 4. a) Real part of the dielectric function $\epsilon_1(\omega)$. b) Imaginary part of the dielectric function $\epsilon_2(\omega)$. c) The refractive index $n(\omega)$. d) The reflectivity $R(\omega)$. e) The optical conductivity $\sigma(\omega)$.

In this study, we computed the optical spectra of $\epsilon(\omega)$ with 50000 k-points in the IBZ. The variations in the real and imaginary parts ($\epsilon_1(\omega)$, $\epsilon_2(\omega)$) of the dielectric function in the energy range of 0-12 eV are plotted in Fig. 4a) and Fig. 4b) respectively. At zero frequency, the static dielectric constant $\epsilon_1(0)$ is 3.20. The real part of the $\epsilon_1(\omega)$ spectrum grows with increasing energy until reaching a maximum value of 5.68 at 3.73 eV. After the peak, the $\epsilon_1(\omega)$ decreases with an increase in energy, becomes negative at 5.97 eV, and then increases at higher energy. The negative values of the $\epsilon_1(\omega)$ idealize the total reflection of the incident photons [46].

It can be seen in Fig. 4b) that the imaginary part has threshold energy at 1.22 eV, which represents the optical transition between VBM and CBM. We can also notice that the maximum absorption is located in the energy range from 4.19 to 6.47 eV, the highest peak intensity of $\epsilon_2(\omega)$ is 5.86 at 5.26 eV. After this point, the $\epsilon_2(\omega)$ spectrum increases.

The refractive index $n(\omega)$ of the Ag_2O compound versus photon energy is shown in Fig. 4c), the static refractive index $n(0)$ is 1.78, which satisfies the relation $n(0) = (\epsilon_1(0))^{1/2}$. We remark that the $n(\omega)$ spectra that reach a maximum peak value of 2.42 at 4.81 eV. Beyond the maximum value, $n(\omega)$ decreases with increasing energy.

The variation in the reflectivity $R(\omega)$ is shown in Fig. 4d), at zero frequency, the reflectivity $R(0)$ is 8.10%, and it is obvious that $R(\omega)$ takes the maximum value (33.60%) at 6.12 eV.

As shown in Fig. 4e), we calculate the optical conductivity $\sigma(\omega)$. In the low-energy range, we can see a drastic decrease owing to the Drude interaction mechanism of light waves with conduction electrons. The maximum value of $\sigma(\omega)$ is 4165.58 $\Omega^{-1}\text{cm}^{-1}$ at 5.27 eV.

4. Conclusion

Herein, we have used the FP-LAPW method based on the DFT-theory to study the effect of different exchange-correlation functionals on the optoelectronic properties of the chalcogenide compound Ag_2O. From the calculated electronic band structure, it was observed that the Ag_2O compound exhibited a direct semiconductor nature with an energy bandgap of 1.22 eV, which agrees with the experimental values for the first time. The study of mechanical stability showed that the compound was stable against elastic deformation. From the obtained elastic moduli, we conclude that our compound is an anisotropic ductile material. The $\epsilon_1(\omega)$ and $\epsilon_2(\omega)$ parts of dielectric functions were estimated to identify optical transitions. $n(\omega)$, $R(\omega)$, and $\sigma(\omega)$ were also obtained and analyzed up to 12 eV. Finally, Ag_2O was found to be useful for optoelectronic applications.

Acknowledgements

The study was supported by grant B00L02UN220120190002 from the DGRSDT (The general directorate for scientific research and technological development).

1. A. Kirfel and K. Eichhorn, Accurate structure analysis with synchrotron radiation. The electron density in Al_2O_3 and Cu_2O, *Acta Crystallographica Section A: Foundations and Advances* **46** (1990) 271, https://doi.org/10.1107/S0108767389012596.

2. A. Gordienko, Y. N. Zhuravlev, and D. Fedorov, Band structure and chemical bonding in Cu_2O and Ag_2O oxides, *Physics of the Solid State* **49** (2007) 223, https://doi.org/10.1134/S1063783407020072.

3. L.-H. Tjeng *et al.*, Electronic structure of Ag_2O, *Physical Review B* **41** (1990) 3190, https://doi.org/10.1103/PhysRevB.41.3190.

4. J. Tominaga, The application of silver oxide thin films to plasmon photonic devices, *Journal of Physics: Condensed Matter* **15** (2003) R1101, https://doi.org/10.1088/0953-8984/15/25/201.

5. D. F. Smith and J. A. Gucinski, Synthetic silver oxide and mercury-free zinc electrodes for silver-zinc reserve batteries, *Journal of power sources* **80** (1999) 66, https://doi.org/10.1016/S0378-7753(98)00251-1.

6. D. F. Smith and C. Brown, Aging in chemically prepared divalent silver oxide electrodes for silver/zinc reserve batteries, *Journal of power sources* **96** (2001) 121, https://doi.org/10.1016/S0378-7753(00)00679-0.

7. J. Pan *et al.*, Nano silver oxide (AgO) as a super high charge/discharge rate cathode material for rechargeable alkaline batteries, *Journal of Materials Chemistry* **17** (2007) 4820, https://doi.org/10.1039/B711373K.

8. H. Li *et al.*, A novel rechargeable Li-AgO battery with hybrid electrolytes, *Chemical communications* **46** (2010) 2055, https://doi.org/10.1039/B923706B.

9. D. Dellasega *et al.*, Nanostructured Ag_4O_4 films with enhanced antibacterial activity, *Nanotechnology* **19** (2008) 475602, https://doi.org/10.1088/0957-4484/19/47/475602.

10. D. Dellasega *et al.*, Nanostructured high valence silver oxide produced by pulsed laser deposition, *Applied surface science* **255** (2009) 5248, https://doi.org/10.1016/j.apsusc.2008.07.170.

11. X. Wang *et al.*, Shape-dependent antibacterial activities of Ag_2O polyhedral particles, *Langmuir* **26** (2010) 2774, https://doi.org/10.1021/la9028172.

12. B. Fang *et al.*, Silver oxide nanowalls grown on Cu substrate as an enzymeless glucose sensor, *ACS applied materials &*

interfaces **1** (2009) 2829, https://doi.org/10.1021/am900576z.

13. W. Wang *et al.*, A novel silver oxides oxygen evolving catalyst for water splitting, *International journal of hydrogen energy* **36** (2011) 7374, https://doi.org/10.1016/j.ijhydene.2011.03.096.
14. M. Fujimaki *et al.*, Surface-enhanced Raman scattering from Ag nanoparticles formed by visible laser irradiation of thermally annealed AgO_x thin films, *Journal of applied physics* **100** (2006) 074303, https://doi.org/10.1063/1.2354329.
15. T. Rollins and F. Weichman, Changes in Ag_2O Films, *physica status solidi (b)* **15** (1966) 233, https://doi.org/10.1002/pssb.19660150122.
16. R. H. Crabtree, NHC ligands versus cyclopentadienyls and phosphines as spectator ligands in organometallic catalysis, *Journal of organometallic chemistry* **690** (2005) 5451, https://doi.org/10.1016/j.jorganchem.2005.07.099.
17. Q. Tian, D. Shi, and Y. Sha, CuO and Ag_2O/CuO catalyzed oxidation of aldehydes to the corresponding carboxylic acids by molecular oxygen, *Molecules* **13** (2008) 948, https://doi.org/10.3390/molecules13040948.
18. S. a Beccara *et al.*, Local thermal expansion in a cuprite structure: The case of Ag_2O, *Physical review letters* **89** (2002) 025503, https://doi.org/10.1103/PhysRevLett.89.025503.
19. A. Sanson *et al.*, Negative thermal expansion and local dynamics in Cu_2O and Ag_2O, *Physical Review B* **73** (2006) 214305, https://doi.org/10.1103/PhysRevB.73.214305.
20. B. J. Kennedy, Y. Kubota, and K. Kato, Negative thermal expansion and phase transition behaviour in Ag_2O, *Solid state communications* **136** (2005) 177, https://doi.org/10.1016/j.ssc.2005.05.043.
21. A. Sanson, A first-principles study of vibrational modes in Cu_2O and Ag_2O crystals, *Solid state communications* **151** (2011) 1452, https://doi.org/10.1016/j.ssc.2011.07.006.
22. K. S. Pitzerr *et al.*, Transitions and thermal anomalies in silver oxide, *Pure and Applied Chemistry* **2** (1961) 211, https://doi.org/10.1351/pac196102010211.
23. Z. Wiśniewski, R. Wiśniewski, and J. Nowiński, Compressibility investigations of AgI-Ag_2O-P_2O_5 superionic materials, *Solid State Ionics* **157** (2003) 275, https://doi.org/10.1016/S0167-2738(02)00221-7.
24. F. Pei *et al.*, Electronic and optical properties of noble metal oxides M_2O (M= Cu, Ag and Au): First-principles study, *Journal of the Korean Physical Society* **55** (2009) 1243, https://doi.org/10.3938/jkps.55.1243.
25. J. P. Allen, D. O. Scanlon, and G. W. Watson, Electronic structures of silver oxides, *Physical Review B* **84** (2011) 115141, https://doi.org/10.1103/PhysRevB.84.115141.
26. H. U. Din and A. Reshak, Structural, elastic, thermal, electronic and optical properties of Ag_2O under pressure, *Computational materials science* **83** (2014) 474, https://doi.org/10.1016/j.commatsci.2013.11.021.
27. N. Umezawa, O. Shuxin, and J. Ye, Theoretical study of high photocatalytic performance of Ag_3PO_4, *Physical Review B* **83** (2011) 035202, https://doi.org/10.1103/PhysRevB.83.035202.
28. E. Sjöstedt, L. Nordström, and D. Singh, An alternative way of linearizing the augmented plane-wave method, *Solid state communications* **114** (2000) 15, https://doi.org/10.1016/S0038-1098(99)00577-3.
29. G. K. Madsen *et al.*, Efficient linearization of the augmented plane-wave method, *Physical Review B* **64** (2001) 195134, https://doi.org/10.1103/PhysRevB.64.195134.
30. P. Hohenberg and W. Kohn, Inhomogeneous electron gas, *Physical review* **136** (1964) B864, https://doi.org/10.1103/PhysRev.136.B864.
31. W. Kohn and L. J. Sham, Self-consistent equations including exchange and correlation effects, *Physical review* **140** (1965) A1133, https://doi.org/10.1103/PhysRev.140.A1133.
32. P. Blaha *et al.*, WIEN2k: An APW+ lo program for calculating the properties of solids, *The Journal of Chemical Physics* **152** (2020) 074101, https://doi.org/10.1063/1.5143061.
33. W. Jiang *et al.*, Systematic research on Ag_2X (X= O, S, Se, Te) as visible and near-infrared light driven photocatalysts and effects of their electronic structures, *Applied Surface Science* **427** (2018) 1202, https://doi.org/10.1016/j.apsusc.2017.08.053.
34. M. Jamal *et al.*, Elastic constants of cubic crystals, *Computational Materials Science* **95** (2014) 592, https://doi.org/10.1016/j.commatsci.2014.08.027.
35. M. Jamal *et al.*, IRelast package, *Journal of Alloys and Compounds* **735** (2018) 569, https://doi.org/10.1016/j.jallcom.2017.10.139.
36. F. Murnaghan, On the theory of the tension of an elastic cylinder, *Proceedings of the National Academy of Sciences of the United States of America* **30** (1944) 382, https://doi.org/10.1073/pnas.30.12.382.
37. R. G Wyckoff, Crystal Structures (1965).
38. K. Z. Yahia, Study Optoelectronic Properties of Ag_2O Heterojunction Prepered by Thermal Oxidation Technique, *Engineering and Technology Journal* **26** (2008) 570.
39. M. H. Elahmar, H. Rached, and D. Rached, The half metallic feature at high temperature of the novel half-Heusler alloys and their [100] oriented layered superlattices: A DFT investigations, *Materials Chemistry and Physics* **267** (2021) 124712, https://doi.org/10.1016/j.matchemphys.2021.124712.
40. H. Rached *et al.*, First-principles study of structural stabilities, elastic and electronic properties of transition metal monocarbides (TMCs) and mononitrides (TMNs), *Materials Chemistry and Physics* **143** (2013) 93, https://doi.org/10.1016/j.matchemphys.2013.08.020.

41. I. Bourachid *et al.*, Insight into the structural, electronic, mechanical and optical properties of inorganic lead bromide perovskite APbBr3 (A= Li, Na, K, Rb, and Cs), *Computational Condensed Matter* **24** (2020) e00478, https://doi.org/10.1016/j.cocom.2020.e00478.

42. A. Azzouz-Rached *et al.*, Prediction of a new Sn-based MAX phases for nuclear industry applications: DFT calculations, *Materials Today Communications* **27** (2021) 102233, https://doi.org/10.1016/j.mtcomm.2021.102233.

43. A. Azzouz-Rached *et al.*, Prediction of double transition metal $(Cr_{1-x}Zr_x)_2AlC$ MAX phases as thermal barrier coatings: Insight from density functional theory, *International Journal of Quantum Chemistry* **121** (2021) e26770, https://doi.org/10.1002/qua.26770.

44. A. Azzouz-Rached *et al.*, Pressure effects on the structural, elastic, magnetic and thermodynamic properties of Mn_2AlC andMn_2SiC MAX phases, *Journal of Alloys and Compounds* **885** (2021) 160998, https://doi.org/10.1016/j.jallcom.2021.160998.

45. C. Ambrosch-Draxl and J. O. Sofo, Linear optical properties of solids within the full-potential linearized augmented planewave method, *Computer physics communications* **175** (2006) 1, https://doi.org/10.1016/j.cpc.2006.03.005.

46. M. Caid *et al.*, High-throughput study of the structural, electronic, and optical properties of short-period (BeSe)m/(ZnSe)n superlattices based on DFT calculations, *Computational Condensed Matter* **29** (2021) e00598, https://doi.org/10.1016/j.cocom.2021.e00598.